Strange Electromagnetic Form Factors of the Nucleon with $N_f = 2 + 1$ $\mathcal{O}(a)$-Improved Wilson Fermions

D. Djukanovic[⬤],[1] K. Ottnad,[1,2] J. Wilhelm,[2] and H. Wittig[1,2]

[1]*Helmholtz Institute Mainz, Staudingerweg 18, D-55128 Mainz, Germany*

[2]*PRISMA+ Cluster of Excellence and Institute for Nuclear Physics, Johannes Gutenberg University of Mainz,*
Johann-Joachim-Becher-Weg 45, D-55128 Mainz, Germany

We present results for the strange contribution to the electromagnetic form factors of the nucleon computed on the coordinated lattice simulation ensembles with $N_f = 2 + 1$ flavors of $\mathcal{O}(a)$-improved Wilson fermions and an $\mathcal{O}(a)$-improved vector current. Several source-sink separations are investigated in order to estimate the excited-state contamination. We calculate the form factors on six ensembles with lattice spacings in the range of $a = 0.049$–0.086 fm and pion masses in the range of $m_\pi = 200$–360 MeV, which allows for a controlled chiral and continuum extrapolation. In the computation of the quark-disconnected contributions, we employ hierarchical probing as a variance-reduction technique.

The contributions of strange sea quarks to the nucleon electromagnetic form factors, which characterize the charge and current distribution in the nucleon, have been of high interest in the last decades. Experimentally, strange electromagnetic form factors can be measured through the parity-violating asymmetry, arising from the interference of the electromagnetic and neutral weak interactions, in the elastic scattering of polarized electrons on unpolarized protons. The first measurement by the SAMPLE experiment, at backward angles and low Q^2, yielded a result for G_M^s which is consistent with zero [1]. The G0 collaboration combined measurements at forward and backward angles and found a first indication of a nonzero G_E^s and G_M^s, contributing $\lesssim 10\%$ to the nucleon electromagnetic form factors [2,3]. A first nonzero measurement has been obtained by the A4 experiment at MAMI with a four momentum transfer squared of $Q^2 = 0.22$ GeV^2, where $G_E^s = 0.050 \pm 0.038 \pm 0.019$ and $G_M^s = -0.14 \pm 0.11 \pm 0.11$ [4]. A recent measurement from the HAPPEX collaboration at $Q^2 = 0.624$ GeV^2 found a value for the combination of the strange electromagnetic form factors consistent with zero $G_E^s + 0.517 G_M^s = 0.003 \pm 0.010 \pm 0.004 \pm 0.009$ [5], confirming a previous measurement at $Q^2 = 0.48$ GeV^2, where a value consistent with zero was found as well [6]. For a recent review of the experimental status of the strange electromagnetic form factors, see [7]. On the theoretical side, lattice QCD simulations allow for a nonperturbative determination of the strange nucleon form factors. This is a challenging calculation, due to the appearance of quark-disconnected diagrams, which are notoriously difficult to evaluate. The most expensive part of the pertinent simulation is the calculation of the trace of an all-to-all propagator. In order to obtain a good signal, the application of variance-reduction techniques, such as hierarchical probing [8], are crucial. A prominent example to illustrate the importance of a precise knowledge of the strange nucleon form factors is the weak charge of the proton. At tree level and without radiative corrections, the weak charge is connected to the weak mixing angle through $Q_W(p) = 1 - 4\sin^2\theta_W$. Hence, through measurements of $Q_W(p)$, one can determine a fundamental parameter of the Standard Model. The experiment proceeds by measuring the parity-violating asymmetry, from which $Q_W(p)$ can be isolated, provided that the required nucleon form factors to describe the hadronic contribution are known [7,9]. Here the strange electromagnetic form factors G_E^s and G_M^s, as well as the strange axial form factor G_A^s, play a crucial role, as they constitute the leading uncertainty. In this Letter, we closely follow the strategy outlined in [10].

We make use of the coordinated lattice simulation (CLS) $N_f = 2 + 1$ $\mathcal{O}(a)$-improved Wilson fermion ensembles with the tree-level-improved Lüscher-Weisz gauge action [11]. The fermion fields have open boundary conditions in time in order to prevent topological freezing [12]. Simulations have been performed such that the sum of the bare quark masses is constant, which implies a constant $\mathcal{O}(a)$-improved coupling [13]. See Table I for a list of ensembles used in this Letter. We obtain the strange electromagnetic form factors of the nucleon by calculating the disconnected three-point function with a vector current insertion in the strange quark loop. The relevant diagram

TABLE I. Gauge ensembles used in this Letter, where N_{cfg} denotes the number of gauge configurations and the last column corresponds to the total number of measurements for the ratio in Eq. (7). The values for the lattice spacing and pion and kaon masses are taken from [14], while the nucleon masses are estimated using the two-point function in this work. For the ensembles marked with an asterisk, the pion and kaon masses have been obtained from dedicated runs in connection with [15].

	β	a (fm)	$N_s^3 \times N_t$	m_π (MeV)	m_K (MeV)	m_N (MeV)	$m_K L$	N_{cfg}	N_{meas}
H105	3.40	0.086 36	$32^3 \times 96$	278	460	1037	6.44	1020	391 680
N401*	3.46	0.076 34	$48^3 \times 128$	289	462	1042	8.59	701	314 048
N203	3.55	0.064 26	$48^3 \times 128$	345	441	1111	6.90	772	345 856
N200	3.55	0.064 26	$48^3 \times 128$	283	463	1061	7.23	856	383 488
D200	3.55	0.064 26	$64^3 \times 128$	200	480	989	10.01	278	124 544
N302*	3.70	0.049 81	$48^3 \times 128$	354	458	1120	5.55	1177	527 296

and our chosen momentum setup is depicted in Fig. 1. The disconnected three-point function factorizes into separate traces for the strange quark loop and the nucleon two-point function

$$C_{3,V_\mu}^s(\boldsymbol{q}, z_0; \boldsymbol{p}', y_0, x; \Gamma_\nu)$$
$$= \langle e^{-i\boldsymbol{q}\boldsymbol{x}} \mathcal{L}_{V_\mu}^s(\boldsymbol{q}, z_0) \cdot C_2(\boldsymbol{p}', y_0, x; \Gamma_\nu) \rangle_G, \quad (1)$$

where $\mathcal{L}^s$ and C_2 denote the strange loop, given in Eq. (4), and the nucleon two-point function, respectively.

The calculation of nucleon two-point function C_2 proceeds via the standard nucleon interpolator

$$N_\alpha(x) = \epsilon_{abc}[u_\beta^a(x)(C\gamma_5)_{\beta\gamma}d_\gamma^b(x)]u_\alpha^c(x), \quad (2)$$

and $\Gamma_0 = \frac{1}{2}(1 + \gamma_0)$, which ensures the correct parity of the nucleon at zero momentum. Wuppertal smearing [16] is applied at the source and the sink for all quark propagators. We increase the statistics of the nucleon two-point function using the truncated solver method [17,18]. Traces over the strange quark loops can be stochastically estimated using four-dimensional noise vectors η. For a local current

$$V^s = \bar{s}(x)\Gamma s(x), \quad (3)$$

the trace over the strange quark loop then reads
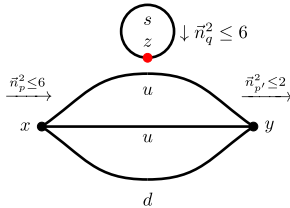
FIG. 1. Disconnected three-point function with a vector current inserted in the strange loop (red dot). For the range of momenta at the source and current insertion, we use $\vec{n}_{p/q}^2 \leq 6$, while at the sink, we restrict the range to $\vec{n}_{p'}^2 \leq 2$ ($\vec{n}_{p/q/p'}^2$ denote the units of squared lattice momenta).

$$\langle \mathcal{L}_\Gamma^s(\boldsymbol{q}, z_0) \rangle_G = -\sum_{z \in \Lambda} e^{i\boldsymbol{q}\cdot z} \langle \text{tr}[S^s(z; z)\Gamma] \rangle_G$$
$$= -\sum_{z \in \Lambda} e^{i\boldsymbol{q}\cdot z} \langle \eta^\dagger(z)\Gamma\psi(z) \rangle_{G,\eta}, \quad (4)$$

with

$$D^s\psi = \eta, \quad (5)$$

where D^s denotes the Dirac operator for the strange quark, and the sum is taken over the spatial volume Λ. Instead of a local current, we consider the $\mathcal{O}(a)$-improved conserved vector current in this Letter

$$V_\mu(z)^{\text{Imp}} = \frac{1}{2}[\bar{s}(z + \hat{\mu}a)(1 + \gamma_\mu)U_\mu(z)^\dagger s(z)$$
$$- \bar{s}(z)(1 - \gamma_\mu)U_\mu(z)s(z + \hat{\mu}a)]$$
$$+ ac_V \partial_\nu(\bar{s}(z)\sigma_{\mu\nu}s(z)), \quad (6)$$

with the improvement coefficient c_V taken from [19]. Furthermore, we use hierarchical probing [8], which replaces the sequence of noise vectors by one noise vector multiplied with a sequence of Hadamard vectors. We find that the statistical error of the strange quark loop is reduced by a factor of 5 when using 512 Hadamard vectors, compared to the estimate based on 512 U(1) noise vectors, for nearly the same cost. The quark loops in this study were obtained by averaging two independent noise vectors with 512 Hadamard vectors each. To extract the strange contribution to the electromagnetic form factors of the nucleon, we consider the ratios (see [20–22])

$$R_{V_\mu}^s(z_0, \boldsymbol{q}; y_0, \boldsymbol{p}'; \Gamma_\nu)$$
$$= \frac{C_{3,V_\mu}^s(\boldsymbol{q}, z_0; \boldsymbol{p}', y_0; \Gamma_\nu)}{C_2(\boldsymbol{p}', y_0)}$$
$$\times \sqrt{\frac{C_2(\boldsymbol{p}', y_0)C_2(\boldsymbol{p}', z_0)C_2(\boldsymbol{p}' - \boldsymbol{q}, y_0 - z_0)}{C_2(\boldsymbol{p}' - \boldsymbol{q}, y_0)C_2(\boldsymbol{p}' - \boldsymbol{q}, z_0)C_2(\boldsymbol{p}', y_0 - z_0)}}. \quad (7)$$

Performing the spectral decomposition and only taking the ground state into account, these ratios read

$$R_{V_\mu}^s(z_0, \boldsymbol{q}; y_0, \boldsymbol{p'}; \Gamma_\nu) \xrightarrow{z_0,(y_0-z_0)\to\infty} \frac{1}{4\sqrt{(E_{\boldsymbol{p'}-\boldsymbol{q}}+m)(E_{\boldsymbol{p'}}+m)E_{\boldsymbol{p'}}E_{\boldsymbol{p'}-\boldsymbol{q}}}} T(\tilde{V}_\mu^s, \Gamma_\nu, \boldsymbol{q}, \boldsymbol{p'}), \tag{8}$$

$$T(\tilde{V}_\mu^s, \Gamma_\nu, \boldsymbol{q}, \boldsymbol{p'}) = \mathrm{tr}[\Gamma_\nu(E_{\boldsymbol{p'}}\gamma_0 - i\boldsymbol{p'}\boldsymbol{\gamma} + m)\tilde{V}_\mu^s(\boldsymbol{q})(E_{\boldsymbol{p'}-\boldsymbol{q}}\gamma_0 - i(\boldsymbol{p'}-\boldsymbol{q})\boldsymbol{\gamma} + m)], \tag{9}$$

where $\tilde{V}_\mu^s$ can be obtained using the parametrization of the nucleon matrix element

$$\langle N, \boldsymbol{k}, s|V^\mu(x)|N, \boldsymbol{k'}, s'\rangle = \bar{u}^s(\boldsymbol{k})\left(\gamma^\mu F_1(Q^2) + i\sigma^{\mu\nu}\frac{q_\nu}{2m}F_2(Q^2)\right)u^{s'}(\boldsymbol{k'})e^{iqx}. \tag{10}$$

We proceed by evaluating the trace in Eq. (9) for four different projectors

$$\Gamma_0 = \frac{1}{2}(1+\gamma_0), \qquad \Gamma_k = \Gamma_0 i\gamma_5\gamma_k, \qquad k \in \{1, 2, 3\}, \tag{11}$$

combined with all components of the vector current $\tilde{V}_\mu^s$, leading to the asymptotic behavior of the ratios in the following form:

$$R_{V_\mu}^s(z_0, \boldsymbol{q}; y_0, \boldsymbol{p'}; \Gamma_\nu) \xrightarrow{z_0,(y_0-z_0)\to\infty} M_{\mu\nu}^E(\boldsymbol{q}, \boldsymbol{p'})G_E^s(Q^2) + M_{\mu\nu}^M(\boldsymbol{q}, \boldsymbol{p'})G_M^s(Q^2). \tag{12}$$

In analogy with Ref. [23], we collect all kinematic prefactors $M_{\mu\nu}^E$ and $M_{\mu\nu}^M$ at a common Q^2 into a matrix M and write the ratios as a vector $\boldsymbol{R}$, which results in a (generally) overdetermined system of equations for the form factors $\boldsymbol{G}$

$$M\boldsymbol{G} = \boldsymbol{R}, \qquad M = \begin{pmatrix} M_1^E & M_1^M \\ \vdots & \vdots \\ M_N^E & M_N^M \end{pmatrix},$$

$$\boldsymbol{G} = \begin{pmatrix} G_E^s \\ G_M^s \end{pmatrix}, \qquad \boldsymbol{R} = \begin{pmatrix} R_1 \\ \vdots \\ R_N \end{pmatrix}. \tag{13}$$

The system can be solved by minimizing the least-squares function

$$\chi^2 = (\boldsymbol{R} - M\boldsymbol{G})^T C^{-1}(\boldsymbol{R} - M\boldsymbol{G}), \tag{14}$$

where C denotes the covariance matrix. Note that we neglect all equations with vanishing kinematical factors ($M^E = M^M = 0$) and average equivalent equations, i.e., with identical M^E and M^M. The latter average can already be carried out at the level of the nucleon three-point functions, where the momenta of the nucleon states at the source and the sink of the three-point functions are related by spatial symmetry [24]. In addition, averaging the nucleon two-point functions over equivalent momentum classes, we construct the ratios in Eq. (7) from these averaged correlation functions. Solving the system of equations at each z_0 and y_0 leads to the so-called effective

form factors, which still suffer from excited-state contamination. Following Refs. [16,25–27], we obtain an estimate of the asymptotic value of the form factors using the summation method with source-sink separations in the range of $y_0 = 0.5$–1.3 fm. In the case of the magnetic form factor, the plateau estimates show a clear trend toward the results obtained using the summation method. For the electric form factor, both methods agree already at small values of y_0. The effective form factors for several source-sink separations are shown in Fig. 2. No significant deviation from a plateau around the midpoint is visible. (We have included the effective mass plot for the nucleon on ensemble N200 in the Supplemental Material [28].)

We will use the summation method data as our standard dataset, since they are less affected by excited-state contamination, compared to the plateau fits. Nevertheless, we include the analysis of the plateau data, for a conservative choice of source-sink separation of 1 fm using 5 points around the midpoint, as an estimate for the uncertainty coming from excited states. In order to further analyze the kaon mass and lattice spacing dependence, we use model-independent z-expansion fits [30,31] to fifth order to extract the radii and magnetic moment. (We have explicitly checked that going to a maximum order of 10 does not change the fit results.) The form factors can be expanded as

$$G_{E/M}(Q^2) = \sum_{k=1/0}^{5} a_k^{E/M} z(Q^2)^k,$$

$$z(Q^2) = \frac{\sqrt{t_{\mathrm{cut}} + Q^2} - \sqrt{t_{\mathrm{cut}}}}{\sqrt{t_{\mathrm{cut}} + Q^2} + \sqrt{t_{\mathrm{cut}}}}. \tag{15}$$
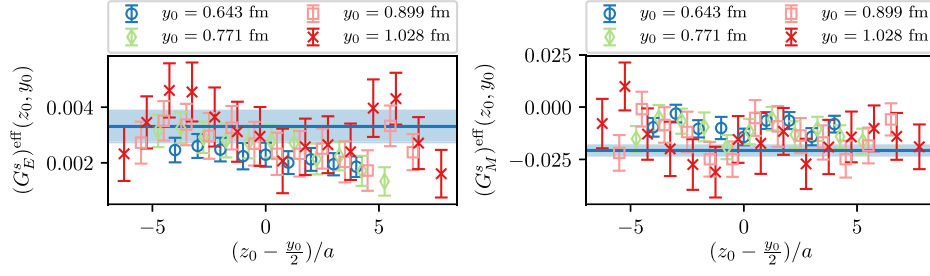
FIG. 2. Results for the effective form factors on ensemble N200 determined via Eq. (13) at $Q^2 = 0.156$ GeV^2 compared to the estimate derived from the summation method (horizontal band).

Since the physical ω and ϕ mesons are narrow resonances and because one cannot easily establish whether or not they are unstable particles on the analyzed ensembles, we use $4m_K^2$ for the value of the cut in the z expansion, where we use the ensemble kaon mass for m_K (see Table I). We stabilize the fits using Gaussian priors centered around zero for all coefficients with $k > 1$. To this end, we first determine the coefficients $a_{0,1}$ from a fit without priors and subsequently use the maximum of these coefficients to estimate the width of the priors, i.e., $a_{k>1} = 0\pm c \times \max\{|a_0|, |a_1|\}$. We find that for $c = 5$ the extraction of the radii and the magnetic moment are stable and lead to consistent results even after applying a cut of $Q^2 < 0.5$ GeV^2. Finally, we estimate the effect of this choice on the final observables by repeating the analysis with the prior width doubled. From the z-expansion fits, we can extract the strange magnetic moment μ^s, as well as the electric and magnetic charge radii $(r_{E/M}^2)^s$,

$$\mu^s = a_0^M, \qquad (16)$$

$$(r_{E/M}^2)^s = -\frac{3}{2t_{\rm cut}} a_1^{E/M}. \qquad (17)$$
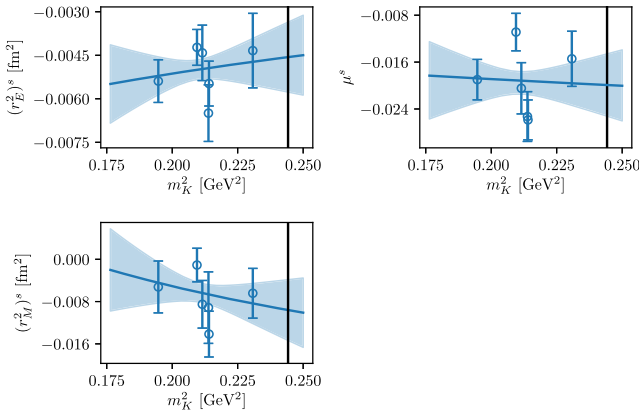
FIG. 3. Chiral and continuum extrapolation of the electric and magnetic radius and magnetic moment, using the standard method of Table II. The vertical line denotes the physical kaon mass in the isospin limit [38].

We have repeated the analysis in several variations in order to assess systematic errors and subsequently perform chiral and continuum extrapolations. Since the radii and magnetic moments are defined at $Q^2 = 0$, we perform the fits applying a cut of $Q^2 < 0.5$ GeV^2 and treat the difference to fitting all of the data as a systematic uncertainty. This cut also ensures that all ensembles contribute over the whole range in Q^2. In total we thus have four sets of values for the radii and magnetic moments for every ensemble, for which we analyze the lattice spacing and kaon mass dependence.

The analyzed set of ensembles allow for a controlled chiral and continuum extrapolation of the strange electromagnetic form factors. In the following, we will investigate the kaon mass dependence using

$$(r_E^2)^s(m_K) = c_1 + c_2 \log(m_K) + \tilde{c}_1 a^2 + c_1^L \sqrt{L} e^{-m_K L},$$

$$\mu^s(m_K) = c_3 + c_4 m_K + \tilde{c}_2 a^2 + c_2^L \left(m_K - \frac{2}{L}\right) e^{-m_K L},$$

$$(r_M^2)^s(m_K) = \frac{c_5}{m_K} + c_6 + \tilde{c}_3 a^2 + c_3^L \sqrt{L} e^{-m_K L}, \qquad (18)$$

which is derived from SU(3) heavy baryon chiral perturbation theory (HBChPT) [32], supplemented by terms describing the dependence on the lattice spacing a and the finite volume. (Note that the CLS ensembles follow the tr$M_q =$ constant trajectory, and so the kaon mass and the pion mass are therefore not varied independently.) Since the finite-volume dependence originates exclusively from kaon loops, we substitute the pion mass in the relevant expression for the magnetic moment [33] by the mass of the

TABLE II. Fit results for the standard fit and variations thereof.

Fit	$(r_E^2)^s$ (fm^2)	μ^s	$(r_M^2)^s$ (fm^2)	$\chi^2/$d.o.f.
Standard	$-0.0046(12)$	$-0.020(5)$	$-0.010(6)$	2.04(12)
Prior width	$-0.0053(15)$	$-0.020(6)$	$-0.012(8)$	1.47(12)
Plateau	$-0.0045(14)$	$-0.022(8)$	$-0.014(8)$	1.62(12)
$\mathcal{O}(a^2)$	$-0.0036(16)$	$-0.009(7)$	$-0.003(8)$	1.91(9)
$\mathcal{O}(\exp[-m_K L])$	$-0.0049(12)$	$-0.021(5)$	$-0.010(6)$	1.12(9)
No cut in Q^2	$-0.0051(9)$	$-0.017(5)$	$-0.008(5)$	3.14(12)
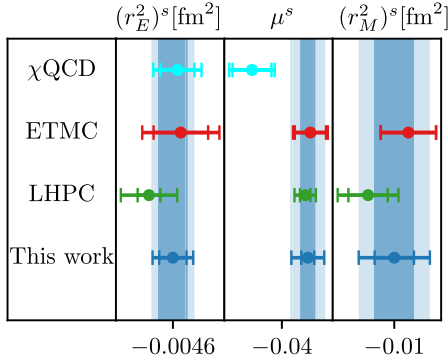
FIG. 4. Comparison of our final values for the radii and magnetic moments with LHPC [42], ETMC [43], and χQCD [34,35], where the dark and light blue bands describe the statistical error and the total error, including systematics, respectively.

FIG. 5. Comparison of our standard fit, based on the z expansion up to $k = 1$, to the analysis of existing experimental data [7]. The dark and light blue bands describe the statistical error and the total error, including systematics, respectively.

$$(r_E^2)_{\text{phys}}^s = -0.0046(12)(7)(1)(9)(3)(6) \text{ fm}^2, \quad (19)$$

$$\mu_{\text{phys}}^s = -0.020(5)(0)(2)(11)(1)(3), \quad (20)$$

$$(r_M^2)_{\text{phys}}^s = -0.010(6)(2)(5)(7)(0)(2) \text{ fm}^2 \quad (21)$$

kaon. For a detailed discussion of the finite-volume dependence, we refer to the Supplemental Material [28]. For the radii, we use the model-dependent ansatz of [34,35], assuming the finite-volume dependence to be same as for the pion form factor calculated in [36], again replacing the pion with the kaon mass. Since our data for the magnetic radius do not show the divergent behavior expected from HBChPT (see Fig. 3), we amend the expressions from [32] by the term c_6. While this cancellation of higher order terms was already found in Ref. [37], we note that the convergence of HBChPT, the rate of which strongly depends on the observable, is, in general, not easily established.

For each of the variations of the z-expansion fit in the previous section, we analyze the chiral behavior separately. The chirally extrapolated values for the standard fit procedure and the variations of the z-expansion fits performed to assess systematic uncertainties are given in Table II. We treat the difference of the central values for the variations as an estimate for a (symmetric) systematic error. In addition, we perform a fit including lattice artifacts or a fit including finite-volume dependence to the standard z-expansion fit. A simultaneous fit of the lattice spacing and finite-volume dependence amounts to the determination of four parameters from six data points for which the AIC_c value is not defined. Therefore, we choose to perform separate extrapolations in our analysis. The AIC_c values, i.e., the Akaike information criterion [39] adjusted for small sample size [40,41], for the fits including lattice spacing or finite-volume effects, are larger by at least 24 in absolute value compared to the minimum AIC_c (for the AIC_c values, we use the maximum likelihood estimator for the sample variance); i.e., the fits omitting $\mathcal{O}(a^2)$, $\mathcal{O}(\exp[-m_K L])$ are favored. We therefore quote the fit without lattice artifacts and finite-volume effects as our best value, using the difference in the central value for the respective procedures as a systematic error from finite lattice spacing and finite-volume corrections. At the physical point, we find

as our final estimate, where the first error is statistical and the remaining errors come from the variations in the fitting procedure given in Table II.

For the radii, our values are in good agreement with other lattice determinations [34,35,42,43]. Our value for the magnetic moment is again in good agreement with [42,43]. The magnetic moment from [34,35] disagrees with our estimate and with [42,43] by more than 2 standard deviations, see Fig. 4. Our best estimate of the radii and magnetic moment compare favorably to the available experimental data, as can be seen from Fig. 5.

In summary, we have reported on our calculation of the strange contribution to the electromagnetic form factors obtained on six CLS $N_f = 2 + 1$ $\mathcal{O}(a)$-improved Wilson fermion ensembles. For the calculation of the disconnected contributions, we use the method of hierarchical probing, which significantly reduces the statistical error. To deal with excited-state contamination, we employ the summation method. We find agreement with plateau estimates for large enough source-sink separations. The strange charge radii and the strange magnetic moment are obtained on each ensemble through model-independent z-expansion fits and later extrapolated to the physical point. See the Supplemental Material [28] for a summary of the extracted form factors and z-expansion fits. Our results are compatible with other lattice QCD studies and in good agreement with experimental data. With the current set of ensembles, the physical values for the strange charge radii and the strange magnetic moment still have large relative statistical errors. We aim to improve this by enlarging the number of ensembles.

[1] D. T. Spayde et al. (SAMPLE Collaboration), Phys. Lett. B 583, 79 (2004).

[2] D. Androić, D. S. Armstrong, J. Arvieux, S. L. Bailey, D. H. Beck, E. J. Beise, J. Benesch, F. Benmokhtar, L. Bimbot, J. Birchall et al. (G0 Collaboration), Phys. Rev. Lett. 104, 012001 (2010).

[3] D. S. Armstrong, J. Arvieux, R. Asaturyan, T. Averett, S. L. Bailey, G. Batigne, D. H. Beck, E. J. Beise, J. Benesch, L. Bimbot et al. (G0 Collaboration), Phys. Rev. Lett. 95, 092001 (2005).

[4] S. Baunack, K. Aulenbacher, D. Balaguer Ríos, L. Capozza, J. Diefenbach, B. Gläser, D. von Harrach, Y. Imai, E.-M. Kabuß, R. Kothe et al., Phys. Rev. Lett. 102, 151803 (2009).

[5] Z. Ahmed, K. Allada, K. A. Aniol, D. S. Armstrong, J. Arrington, P. Baturin, V. Bellini, J. Benesch, R. Beminiwattha, F. Benmokhtar et al. (HAPPEX Collaboration), Phys. Rev. Lett. 108, 102001 (2012).

[6] K. A. Aniol et al. (HAPPEX Collaboration), Phys. Rev. C 69, 065501 (2004).

[7] F. E. Maas and K. D. Paschke, Prog. Part. Nucl. Phys. 95, 209 (2017).

[8] A. Stathopoulos, J. Laeuchli, and K. Orginos, arXiv: 1302.4018.

[9] D. Becker et al., Eur. Phys. J. A 54, 208 (2018).

[10] D. Djukanovic, H. Meyer, K. Ottnad, G. von Hippel, J. Wilhelm, and H. Wittig, Proc. Sci., LATTICE2018 (2018) 118 [arXiv:1810.10810].

[11] M. Bruno, D. Djukanovic, G. P. Engel, A. Francis, G. Herdoiza, H. Horch, P. Korcyl, T. Korzec, M. Papinutto, S. Schaefer et al., J. High Energy Phys. 02 (2015) 043.

[12] M. Lüscher and S. Schaefer, J. High Energy Phys. 07 (2011) 036.

[13] W. Bietenholz, V. Bornyakov, N. Cundy, M. Göckeler, R. Horsley, A. Kennedy, W. Lockhart, Y. Nakamura, H. Perlt, D. Pleiter et al., Phys. Lett. B 690, 436 (2010).

[14] M. Bruno, T. Korzec, and S. Schaefer, Phys. Rev. D 95, 074504 (2017).

[15] M. Cè, A. Gérardin, K. Ottnad, and H. B. Meyer, Proc. Sci., LATTICE2018 (2018) 137 [arXiv:1811.08669].

[16] S. Güsken, Nucl. Phys. B, Proc. Suppl. 17, 361 (1990).

[17] G. Bali, S. Collins, A. Frommer, K. Kahl, I. Kanamori, B. Müller, M. Rottmann, and J. Simeth, Proc. Sci., LAT-TICE2015 (2015) 350 [arXiv:1509.06865].

[18] E. Shintani, R. Arthur, T. Blum, T. Izubuchi, C. Jung, and C. Lehner, Phys. Rev. D 91, 114511 (2015).

[19] A. Gérardin, T. Harris, and H. B. Meyer, Phys. Rev. D 99, 014519 (2019).

[20] C. Alexandrou, T. Korzec, G. Koutsou, M. Brinet, J. Carbonell, V. Drach, P.-A. Harraud, and R. Baron (European Twisted Mass Collaboration), Proc. Sci., LATTICE2008 (2008) 139 [arXiv:0811.0724].

[21] J. R. Green, J. W. Negele, A. V. Pochinsky, S. N. Syritsyn, M. Engelhardt, and S. Krieg, Phys. Rev. D 90, 074507 (2014).

[22] S. Capitani, M. Della Morte, D. Djukanovic, G. von Hippel, J. Hua, B. Jäger, B. Knippschild, H. B. Meyer, T. D. Rae, and H. Wittig, Phys. Rev. D 92, 054511 (2015).

[23] S. Capitani, M. Della Morte, D. Djukanovic, G. M. von Hippel, J. Hua, B. Jäger, P. M. Junnarkar, H. B. Meyer, T. D. Rae, and H. Wittig, Int. J. Mod. Phys. A 34, 1950009 (2019).

[24] S. N. Syritsyn, J. D. Bratt, M. F. Lin, H. B. Meyer, J. W. Negele, A. V. Pochinsky, M. Procura, M. Engelhardt, P. Hägler, T. R. Hemmert et al. (LHPC Collaboration), Phys. Rev. D 81, 034507 (2010).

[25] L. Maiani, G. Martinelli, M. L. Paciello, and B. Taglienti, Nucl. Phys. B293, 420 (1987).

[26] T. Doi, M. Deka, S.-J. Dong, T. Draper, K.-F. Liu, D. Mankame, N. Mathur, and T. Streuer, Phys. Rev. D 80, 094503 (2009).

[27] B. B. Brandt, S. Capitani, M. Della Morte, D. Djukanovic, J. Gegelia, G. von Hippel, A. Jüttner, B. Knippschild, H. B. Meyer, and H. Wittig, Eur. Phys. J. ST 198, 79 (2011).

[28] See Supplemental Material at http://link.aps.org/supplemental/10.1103/PhysRevLett.123.212001 for a detailed discussion of the finite-volume effects, which includes Ref. [29], the effective mass plot of the nucleon for the ensemble N200, and summary tables of the extracted form factors and z-expansion fits for every ensemble.

[29] V. Bernard, N. Kaiser, and U.-G. Meißner, Int. J. Mod. Phys. E 04, 193 (1995).

[30] R. J. Hill and G. Paz, Phys. Rev. D 82, 113005 (2010).

[31] Z. Epstein, G. Paz, and J. Roy, Phys. Rev. D 90, 074027 (2014).

[32] T. R. Hemmert, B. Kubis, and U. G. Meißner, Phys. Rev. C 60, 045501 (1999).

[33] S. R. Beane, Phys. Rev. D 70, 034507 (2004).

[34] R. S. Sufian, Y.-B. Yang, A. Alexandru, T. Draper, J. Liang, and K.-F. Liu, Phys. Rev. Lett. 118, 042001 (2017).

[35] R. S. Sufian, Y.-B. Yang, J. Liang, T. Draper, and K.-F. Liu, Phys. Rev. D 96, 114504 (2017).

[36] B. C. Tiburzi, Phys. Rev. D 90, 054508 (2014).

[37] H. W. Hammer, S. J. Puglia, M. J. Ramsey-Musolf, and S.-L. Zhu, Phys. Lett. B 562, 208 (2003).

[38] S. Aoki et al., Eur. Phys. J. C 77, 112 (2017).

[39] H. Akaike, in Proceedings of the 2nd International Symposium on Information Theory, Akademiai Kiado, Budapest, 1973, edited by B. N. Petrov and F. Csaki (Akademiai Kiado, Budapest, 1973), pp. 267–281.

[40] N. Sugiura, Commun. Stat. 7, 13 (1978).

[41] C. M. Hurvich and C.-L. Tsai, Biometrika **76**, 297 (1989).

[42] J. Green, S. Meinel, M. Engelhardt, S. Krieg, J. Laeuchli, J. Negele, K. Orginos, A. Pochinsky, and S. Syritsyn, Phys. Rev. D **92**, 031501(R) (2015).

[43] C. Alexandrou, M. Constantinou, K. Hadjiyiannakou, K. Jansen, C. Kallidonis, G. Koutsou, and A. V. Avilés-Casco, Phys. Rev. D **97**, 094504 (2018).

[44] R. G. Edwards and B. Joo (SciDAC, LHPC, and UKQCD Collaborations), Nucl. Phys. B, Proc. Suppl. **140**, 832 (2005).

[45] M. Lüscher and S. Schaefer, Comput. Phys. Commun. **184**, 519 (2013).

[46] D. Djukanovic, https://doi.org/10.1016/j.cpc.2019.106950.